ORGANIC PROCESS RESEARCH & DEVELOPMENT
OPR&D

pubs.acs.org/OPRD

Article

Additive Manufacturing as a Rapid Prototyping and Fabrication Tool for Laboratory Crystallizers—A Proof-of-Concept Study

Nico Nys,* Michael König, Peter Neugebauer, Matthew J. Jones, and Heidrun Gruber-Woelfler*

Cite This: *Org. Process Res. Dev.* 2023, 27, 1455−1462

Read Online

ACCESS | Metrics & More | Article Recommendations

ABSTRACT: While large-scale crystallizer design profits from many years of accumulated knowledge, traditional fabrication technologies limit the possibilities for easy and rapid lab-scale design, fabrication, and subsequently testing of crystallizer design variants. Additive manufacturing (three-dimensional (3D) printing) affords an opportunity to overcome the challenges associated with scaling down equipment using traditional fabrication technologies and materials of construction such as glass or metal alloys. Moreover, additive manufacturing provides flexibility in design and the ability to rapidly redesign and prototype novel designs, limited, perhaps, only by the suitability of available materials of construction. Surprisingly, this technology has not yet found widespread use in crystallizer design. In this contribution, we present a concept study for a 3D-printed prototype crystallizer. We discuss additive manufacturing as a tool for rapid design and fabrication of down-scaled crystallizers based upon a design using the classic Oslo-type crystallizer as a starting point. The initial crystallizer design and fabrication process, subsequent design modifications, and investigation of the crystallizer characteristics are discussed here with a view to applications in pharmaceutical continuous crystallization.

KEYWORDS: *continuous crystallization, additive manufacturing, rapid prototyping, in-process analytical technologies*

INTRODUCTION

Manufacturing in the pharmaceutical industry traditionally has been dominated by labor-intensive batch manufacturing, which, by nature, has greater potential for scale-up issues when transferring from the laboratory scale to manufacturing scale compared to continuous manufacturing. Moreover, the greater need for human intervention increases the risk of operator-dependent inconsistencies and human error, a risk that decreases with increasing automation. Therefore, current developments in industry aim at greater automation, efficiency, and use of existing knowledge and data ("Industry 4.0", "end-to-end manufacturing", "machine learning") are becoming increasingly important in the pharmaceutical industry.

While the advantages of continuous manufacturing and automation have been recognized in the pharmaceutical industry, implementation and routine use of such processes have reached different levels of maturity in different parts of the manufacturing workflow from the raw materials to the finished drug product. Continuous manufacturing appears to be more advanced in drug product manufacturing than in drug substance manufacturing.[1−3] While continuous technologies have been subject to research and development in drug substance manufacturing for over two decades, they are far from routine when it comes to their industrial application. Continuous reaction technologies are invaluable for syntheses that are difficult or impossible to handle in batch reactors.[4−7] In crystallization technology, which is the dominant unit operation for isolation and purification of small-molecule drug substances and intermediates, continuous technologies have made limited impact. Mixed suspension mixed product removal (MSMPR) crystallizers are of interest since existing batch crystallizers can easily be repurposed as MSMPRs with limited investment and their heat transfer and flow properties are similar to batch reactors.[8] Plug flow crystallizers have been studied in the context of crystallizing active pharmaceutical substances.[9−12] These are tubular crystallizers typically operated in the plug (laminar) flow regime, which minimizes back-mixing[13] and allows parcels of material to be identified, if required. However, these types of crystallizers are limited in terms of scalability: significantly increasing the tube diameter changes heat transfer and flow properties with potential detrimental effects on the crystallization process. If higher throughputs are demanded, it is advantageous to scale the number of crystallizers rather than scaling the crystallizer itself.[14] A significant body of work is available concerning new concepts for continuous crystallization of pharmaceutically active compounds. Novel crystallizer (proto-)types are, for example, the continuous oscillatory baffled crystallizer,[15] the Archimedes tube crystallizer,[16] and the Taylor Couette flow crystallizers[17] to mention a few.

For the development of novel crystallizer geometries with tailored flow and heat transfer behavior, the application of additive manufacturing affords the opportunity to accelerate

Received: April 25, 2023
Published: July 25, 2023

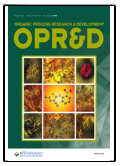

prototyping. The three-dimensional (3D)-printing technology is already well established in micro- and flow-reactor technology, where the precision of 3D printing facilitates printing of customized geometries for static mixing, flow chemistry, and other applications. It has been recognized previously that flexibility of process equipment design, which is considered one of the greatest benefits of additive manufacturing, is a key feature for optimal production systems in the future.[18] In addition to the relevance of this flexibility for technical characteristics, it also has benefits from an economic point of view, where flexibility and speed are required when responding to changing demands for future production capacity.[19]

The ease with which 3D-printed parts can be designed and speed of printing is unprecedented. Even taking into account additional post-printing treatments, such as curing and refining steps (e.g., annealing or polishing, removal of supporting structures[20]), which are frequently required, there is a significant advantage in using this technology in favor of more traditional manufacturing methods. Insufficiently refined parts of crystallizers might lead to undesired effects such as fouling due to excessive surface roughness or undesired heterogeneous nucleation.

Additive manufacturing has been employed in the manufacturing of crystallizers previously.[21,22] To the best of our knowledge, there is no literature on coupling additive manufacturing with a modular approach to equipment design though. Here, we demonstrate that this approach allows design changes to be implemented rapidly and with greater flexibility than possible with traditional equipment manufacturing techniques, in a more sustainable manner as only those parts modified need to be re-fabricated, and at lower cost.

Materials of construction are a critical factor when considering this manufacturing method for constructing equipment for chemical processes. In addition to common polymers, highly heat- and chemical-resistant polymers, stainless steel, and ceramics can be 3D-printed.[23] This adds to the attractiveness of this method for prototype development in the chemical industry.

In addition to the crystallizer designs mentioned above, a number of different designs have been in use for many decades in bulk and commodity chemicals manufacturing. Forced circulation, draft tube baffled, and the OLSO crystallizer are large-scale crystallizers used for the production of inorganic salts, which raises the question whether those concepts can be adapted and applied for the purification and separation of APIs.[24]

In this contribution, we present the application of additive manufacturing for the design of a crystallizer that can be used for the small-scale production of APIs, together with the characterization of pertinent properties of the equipment.

The initial design of the crystallizer was inspired by the OSLO-type circulation/evaporation crystallizer, shown in Figure 1, for several reasons. On the one hand, this is an established crystallizer in large-scale crystallization of commodity chemicals;[25] on the other hand, and to the best knowledge of the authors, laboratory-scale models of this crystallizer are not readily available. Moreover, it contains no moving parts and achieves a fluidized bed of particles by directing the flow through a draft tube to the bottom of the crystallizer, which has a geometry suitable for redirecting the flow of the incoming stream upwards and into the body of the crystallizer, maintaining a fluidized bed therein. Guided by the availability of a significant number of publications on the crystallization of acetylsalicylic acid (ASA) in continuous tubular crystallizers,[26] this compound was selected for the initial characterization of the prototype developed. Ethanol was selected as the solvent due to a reasonable temperature dependence of the solubility and the wide metastable zone width of ASA in that solvent (vide infra).

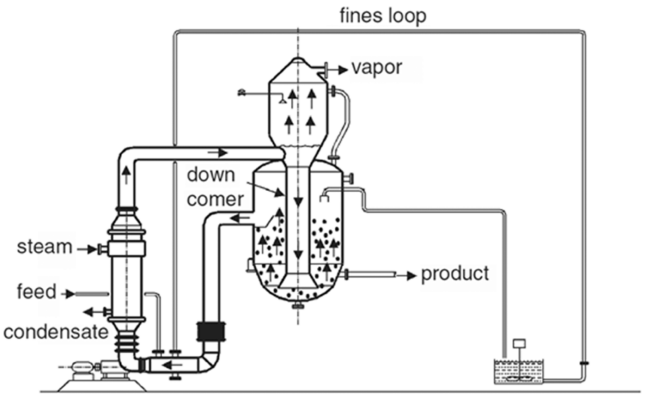

Figure 1. Scheme of an industrial OSLO crystallizer. Reproduced with permission of the licensor through PLSclear from A. Myerson, D. Erdemir, and A. Y. Lee (eds.), Handbook of Industrial Crystallization.[24]

In our approaches focusing on the crystallization of acetylsalicylic acid via cooling crystallization, we could show that the novel crystallizer is a promising alternative to currently prominent designs and unlocks a different approach to the crystallization and product control of APIs.

METHODS AND MATERIALS

Crystallizer Manufacturing Process. *Inventor* (Autodesk) was used to generate the design drawings of the crystallizer modules. The 3D files were positioned and sliced using the *Preform* software (Version 3.16.0, Formlabs). Support structures and printer properties are automatically set by the software. To manufacture the reactor components, the *Form 3* stereolithographic 3D printer (Formlabs) at the lowest possible layer height of 25 μm was used together with the "high temp resin" (Formlabs). The combination of printer and resin delivers sufficiently high resolution to produce a smooth surface, and the cured resin has the required thermal stability and chemical resistance against the solvents to be used in initial tests (water and ethanol). Depending upon the curing conditions, the components are dimensionally stable up to approximately 238 °C.

After the printing process, the supports were removed and the part was rinsed with ethanol and water to remove excess resin from the surface. In order to increase the thermal and chemical resistance, the parts were post-cured using UV light at 60 °C for 30 min in a curing station (Formlabs). These parameters were chosen as longer curing resulted in brittleness of the parts, preventing tight seals between the individual parts of the assembly.

Materials. Acetylsalicylic acid was purchased from Novacyl (>99%). Ethanol was acquired from Carl Roth (>99.8%). Methylene blue used for residence time measurements was purchased from Merck (>99%).

Solubility Measurements. A dynamic solubility measurement method with turbidimetric detection of the dissolution of solids upon heating and nucleation of particles upon cooling

https://doi.org/10.1021/acs.oprd.3c00126
Org. Process Res. Dev. 2023, 27, 1455−1462

was employed. Experiments were carried out in an automated parallel reactor (Crystal16, Technobis).

Slurries of ASA in ethanol with different compositions were prepared in 2 mL glass vials and sealed. All samples were prepared by weight. Samples were agitated and heated from 5 °C to 50 °C and then cooled to 5 °C using a constant rate of 0.01 K min^{-1}. Two temperature cycles were employed. The average temperature from both cycles at which maximum light transmission (complete dissolution) was reached was taken as the solubility at that composition. The temperature at which light transmission begins to decrease was taken as the nucleation temperature and was not averaged.

Figure 2 shows the solubility data obtained together with a fit of the data to an exponential function and the nucleation temperatures. The data match values found in the literature[27] well.

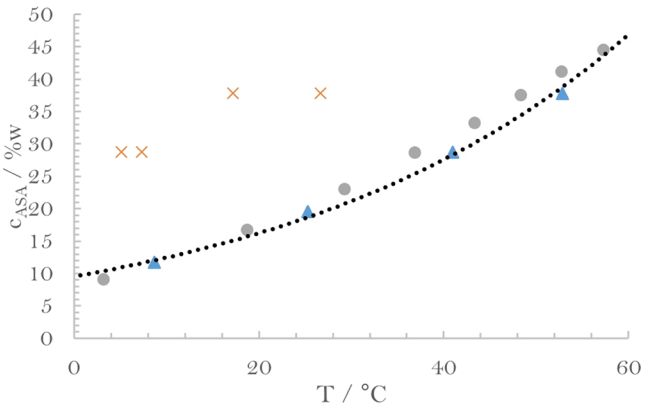

Figure 2. Solubility and nucleation temperatures (line) of acetylsalicylic acid in ethanol. ▲—solubility, ×—nucleation temperatures, dotted line—fit to the solubility data, experimentally obtained. Fit equation: $c^* = 9.522 \exp(0.027T)$, $R^2 = 0.995$. Solubility data from the literature[27] are presented for comparison (●).

Experimental Setup. The crystallizer is arranged within a setup consisting of several pumps and measurement devices. Figure 3 shows the general setup used for the experimental characterization and performance tests of the crystallizer. Depending upon the exact purpose of each experiment, different analytical tools were included. Peristaltic pumps were used for feeding and recirculation (Ismatec IP65, Ismatec Reglo). The feed and product discharge were controlled by the same pump using a single pump head capable of holding several tubes, to ensure a constant volume of liquid in the crystallizer. A thermostat (RP 245 E, Lauda), a thermometer (electronic thermometer, Precision) to track the internal temperature of the crystallizer, and a temperature-controlled (C-MAG HS7, IKA) feed vessel were used for thermal control. For collecting product crystals, a Nutsche filter equipped with standard filter paper was used.

Liquid Phase Residence Time Distribution Measurements. The residence time distribution (RTD) of the liquid phase was determined by observing the propagation of a tracer dye pulse introduced into the reactor. For this purpose, the crystallizer was filled with ethanol (99.8%, Carl Roth) first, then a solution of 120 mg L^{-1} methylene blue (Merck, >99%) in ethanol was used as an inert tracer.

The change in absorption and thus the concentration of the tracer was measured with absorption sensors, which were attached to the feed and outlet tubes. The sensors were

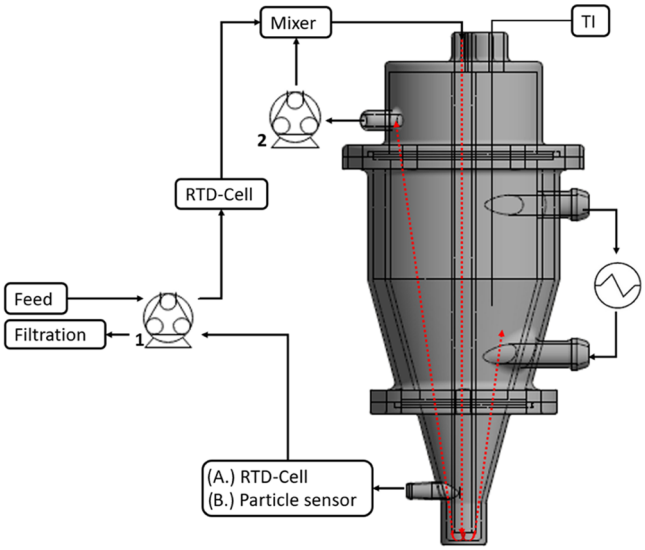

Figure 3. Flow scheme of the experimental setup consisting of a crystallizer, thermostat, peristaltic pump for recirculation (2), peristaltic pump for feed and product withdrawal (1), and sensors for data acquisition. Depending upon the respective experimental investigations, either light absorbance sensors (A, RTD measurements) or a particle sensor (B, particle RTD measurements, crystallization experiments) were included. The red lines indicate general liquid phase flow directions. For details on the crystallizer design, see the Results and Discussion section.

developed in-house and have been presented elsewhere.[28] Measurements of the residence time distribution were performed at feed rates of 10 and 23 mL min^{-1}. The rate of recirculation was adjusted to values between 150 and 320 mL min^{-1} to evaluate the influence of changes in mixing intensity inside the crystallizer.

Particle RTD Measurements. Due to the slow flow velocities of the liquid phase in the flow cell, the movement of the particles is strongly influenced by gravity. Hence, the residence time of the particles had to be determined separately depending upon their individual size, based on the number of particles present in the product stream at each time point measured.[29] A particle sensor (Laser distance sensor (LDS)—70/70, KLOTZ) for particle size measurements[10] was integrated into the product stream. This sensor monitors the particle size distribution by measurement of the signal changes on a photodiode based on the scattering of light by passing particles and therefore reduction of the signal. The particle size is calculated based on the signal reduction.

Seed crystals were prepared from commercial ASA via milling (ball mill, PM100, Retsch) and subsequent sieving. The seed crystal fractions were characterized by means of image analysis in the dry state using a QICPIC device (Sympatec) and suspended in a saturated ASA-EtOH solution, using the particle sensor (KLOTZ).

For measuring the particle RTD, the crystallizer was filled with a saturated solution of ASA in ethanol at ambient temperature. Then, a pulse of seed particles (sieve fraction 50–400 μm, 30 g L^{-1}) was fed into the crystallizer at rates of 10 and 16 mL min^{-1} from a homogeneously stirred feed vessel, which prevents settling of larger particles and therefore ensures equal representations of each crystal size class and the number and size of particles in the product stream was determined.

https://doi.org/10.1021/acs.oprd.3c00126
Org. Process Res. Dev. 2023, 27, 1455−1462

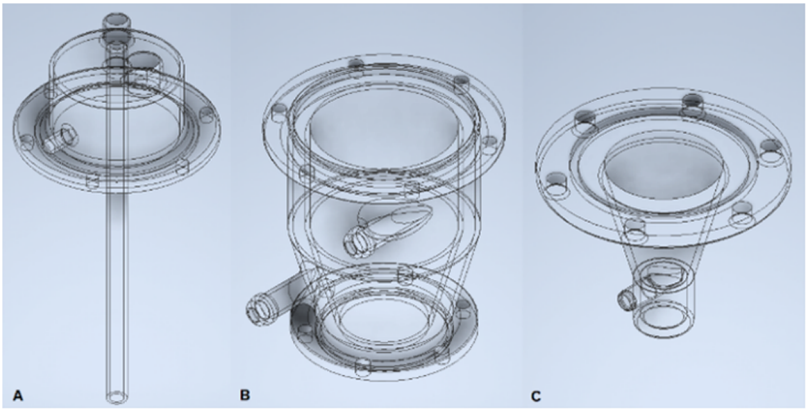

Figure 4. Final design of the crystallizer modules. (A) Top part (including feed pipe, sensor ports, and drain for recirculation), (B) middle part (including double jacket for temperature adjustment), (C) bottom part (conical design including drain for product withdrawal).

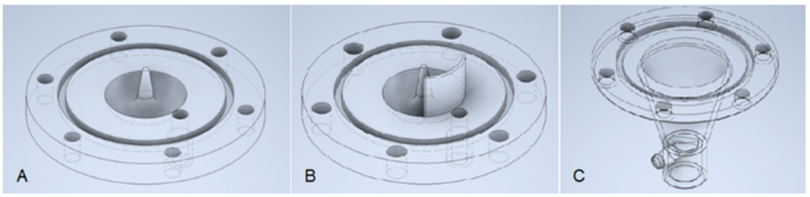

Figure 5. Evolutionary design steps taken for designing the bottom part of the crystallizer: Hemisphere-shaped cavity + central pin (A), hemisphere-shaped cavity + central pin + baffle plate (B), conical extension with flat bottom (C).

Crystallization Experiments. Prior to initiating the crystallization process, a standard procedure for the start-up of the crystallizer was employed. The feed suspension was prepared by generating a saturated solution of ASA in ethanol at the desired feed temperature (28 °C, 20.3% w/w ASA) and then filled into the crystallizer. The internal temperature of the crystallizer was set to 27 °C, which was measured by means of a thermometer inserted through the top port and positioned at the upper edge of the conical part of the crystallizer. Therefore, this temperature is assumed to represent the mean temperature over the height of the crystallizer, since it is located approximately in the center of the equipment. Seed particles (50−100 μm) were added to the feed vessel to a mass loading of 15 g L^{-1}.

The crystallizer jacket temperature was set to the feed temperature via a thermostat (Pro RP 245 E, LAUDA) to prevent nucleation during filling the crystallizer. Once the crystallizer was completely filled, recirculation, feed, and suspension withdrawal rates were set using the peristaltic pumps, and the temperature was set to the desired crystallization temperature. The product particle size distribution was monitored online using the KLOTZ particle sensor. Once the x_{10}, x_{50}, and x_{90} values remained constant over 5 min, i.e., the steady state had been reached, the experiment was terminated.

In addition, product particles were collected on filter paper (Whatman, Grade. 1) and dried overnight at ambient temperature in a desiccator. The filtered and dried particles were analyzed by image analysis (QICPIC).

RESULTS AND DISCUSSION

Design. The crystallizer was designed as a three-module assembly (Figure 4). While industrial OSLO crystallizers consist of an upper segment for evaporation of the solvent and a lower segment for crystallization in a fluidized bed, the design presented in this work was envisaged as a cooling crystallizer for the purpose of prototyping and laboratory experiments.

The main body was designed as a jacketed segment with an inlet and outlet for the cooling/heating medium. The upper part of this module is cylindrical, while the lower part is conical. The crystallizer is completed by two further segments, which are connected by flanges integrated into the design of the respective components. The flanges contain a recess for circular gaskets to ensure a liquid-tight connection.

The upper module consists of a lid with feed inlet, integrated ports for the introduction of probes and sensors (e.g., for temperature or pH measurements), a port for seed crystal addition, and an overflow, allowing partial recirculation of the content of the crystallizer. The inlet is connected to a dip-tube, which extends into the conical section of the crystallizer, ending above the bottom plate of the bottom segment, ensuring convective mixing in the crystallizer.

The lower module contains a port for product removal and is designed to deflect the flow of the feed entering through the dip-tube upward to ensure the formation of a fluidized bed with suitable classification of the particles: Those product particles within the desired product size range settle and are removed through the product removal port. Other particles remain in the fluidized bed until grown to the desired product particle size.

The design of the bottom plate is critical in creating the required flow within the bulk volume of the crystallizer, ensuring low turbulence disturbance to the fluidized bed. During the design phase and subsequent performance tests, three evolutionary steps were taken to realize tailored flow conditions.

The initial geometry shown in Figure 5A contained a hemisphere-shaped cavity and a central pin, intended to redirect the flow of the feed upward. Experimental runs showed that using this initial design, significant amounts of the

https://doi.org/10.1021/acs.oprd.3c00126
Org. Process Res. Dev. 2023, 27, 1455−1462

feed slurry immediately exited the crystallizer through the bottom drain without entering the bulk volume. This negatively affected the average particle residence time and flow velocities impeding the formation of the fluidized bed.

On the basis of these results, a baffle plate was designed between the feed pipe and the product discharge (Figure 5B) to mitigate this problem. This approach was partially successful. Although more particles were initially redirected to the growth zone of the crystallizer, most of the solid material was flushed out rapidly and no fluidized bed was developed.

Unsatisfactory designs A and B of the bottom module stimulated a thorough revision to realize a wider range of flow velocities inside the fluidized bed and to increase the upward flow velocity close to the bottom drain. Hence, design C featured a continuation of the central module's conical section, increasing the total volume of the crystallizer to 340 cm^3. In the course of this change, the top module was redesigned to contain an elongated dip-tube to ensure feed transport to the very bottom of the bottom module.

The currently last stage of evolution of the complete crystallizer, which was used for all subsequent experiments presented in this work, is shown in Figure 6.

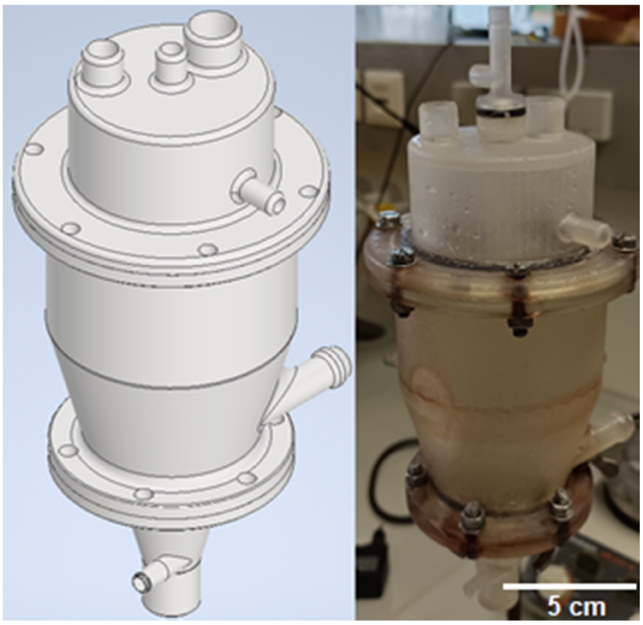

Figure 6. Final design of the fluidized bed crystallizer. Comparison between the technical drawing (left) and the realized 3D-printed prototype already equipped with the mixing element.

The dimensions of the crystallizer are summarized in Table 1.

Table 1. Important Dimensions of the Crystallizer

dimension	
inner diameter cylinder	60 mm
minimum diameter cone	14 mm
maximum diameter cone	60 mm
height cylinder	85 mm
height cone	106.5 mm
inner diameter dip-tube	7 mm
volume	340 mL

Crystallizer Characterization. By integrating the recirculation pump, the flow rate in the fluidized bed was decoupled from the average residence time of the liquid phase. We aimed to identify suitable pump rates for feed and recirculation to realize the formation of a fluidized bed, capable of classifying particles inside the crystallizer according to their settling velocity. Both flushing out seeds through the recirculation port and clogging of the product discharge port by the formation of excessively large product particles need to be avoided.

The Bodenstein number Bo was calculated according to literature[30] to quantify the degree of back-mixing inside the crystallizer. Over the course of all experiments (feed rates 10.3−23.3 mL min^{-1}, recirculation rates: 150−320 mL min^{-1}), the values determined for the Bodenstein number ranged from 2.6 to 4.6, indicating stirred-tank-like behavior.[30] This is explained by the fact that recirculation of the solution leads to a high mixing and homogenization of the internal crystallizer volume, leading to low Bodenstein numbers. Corresponding average residence times of the liquid phase were 200 s for feed rates of 23.3 mL min^{-1}, and 580 s for rates of 10.3 mL min^{-1}. Though the rather short average residence times indicate a quick exchange of the liquid phase from the crystallizer, the fluid behavior deviates from this impression. By inducing the tracer into the crystallizer via the dip-tube, a part of the solution is flushed through the outlet immediately. This results in a rapid increase of the signal at the beginning of the experiment, leading to a short average residence time. Reaching the equilibrium between signal intensity in the feed and product discharge depends upon the experimental conditions and takes 37 min at higher feed rates and up to 60 min at lower feed rates. This indicates that the total exchange of the crystallizer volume takes far longer than initially indicated by the short, average liquid phase residence times.

The average residence time of the particles was calculated for different size classes from particle PSD measurements. Figure 7 shows the dependence of the residence time of the particles upon their size and upon the circulation rate. A low recirculation rate of 245 mL min^{-1} results in the largest difference in residence time when comparing small and large particles. A further increase in the rate of recirculation increases the residence time of larger particles more significantly than for smaller particles. At 350 mL min^{-1} recirculation rate, all particles exit the crystallizer after similar times, indicating that the fluidized bed is fully homogenized and no more classification effects occur.

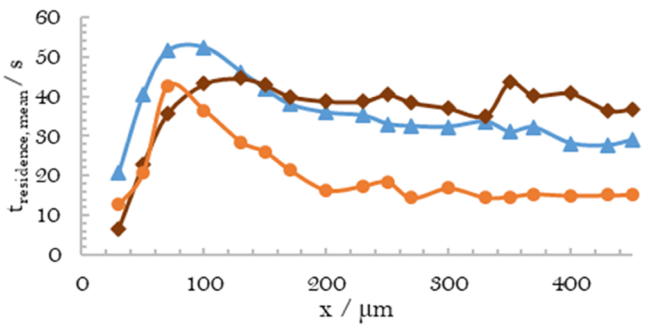

Figure 7. Average residence time of particle sizes x obtained from experiments at 16 mL min^{-1} feed rate and three different recirculation rates: 245 mL min^{-1} (●), 290 mL min^{-1} (▲), 350 mL min^{-1} (◆).

https://doi.org/10.1021/acs.oprd.3c00126
Org. Process Res. Dev. 2023, 27, 1455−1462

For further evaluation, three distinct size classes of crystals were tracked during experiments at 10 and 16 mL min^{-1}, in order to compare the influence of both the feed flow rate and the recirculation rate on the average residence time of the solid phase inside the crystallizer.

The product crystal size should be significantly larger than the seed particle size, and particles with a diameter of 250 μm, in addition to those with size at the lower and upper limits of the seed particles, were selected for the purpose of further evaluation of the performance of the crystallizer.

Figures 8 and 9 show plots of the dependence of the average residence time of particle size classes of interest (50−100 μm

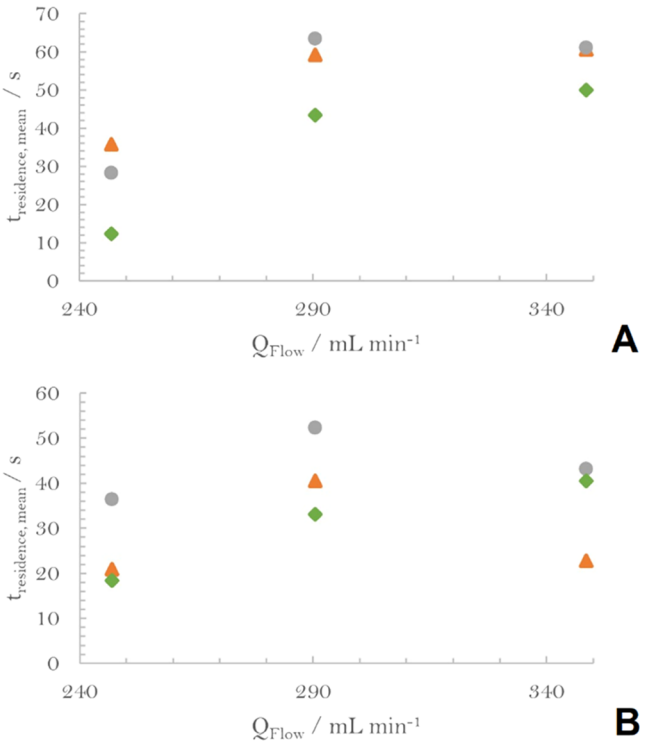

Figure 8. Flow rate of the recirculation pump vs. average residence time for particle sizes of the seed crystals with size between 50 μm (▲) and 100 μm (●), as well as for desired product particles with a size of 250 μm (◆). The feed and product withdrawal rate were kept constant at 10 mL min^{-1} (A) and 16 mL min^{-1} (B).

representing the seeds and 250 μm representing the desired product particle size) upon the flow rate of the recirculation pump at two different feed rates.

According to our experimental validations, the residence time for smaller particles is higher than that for the larger product fraction for all flow rates. This is beneficial for the operation of the crystallizer since the smaller particles should experience an extended growth phase in order to grow into the required, larger product crystals. The most significant increase in residence time can be observed by increasing the recirculation rate from about 245 to 290 mL min^{-1}. This is related to the increased flow velocity at locations closer to the outlet. A further increase of the flow velocity results only in marginal further increases in residence time.

It is assumed that the particles are already suspended at the point of the lowest flow velocity, and therefore no change in the residence time of the particles can be observed.

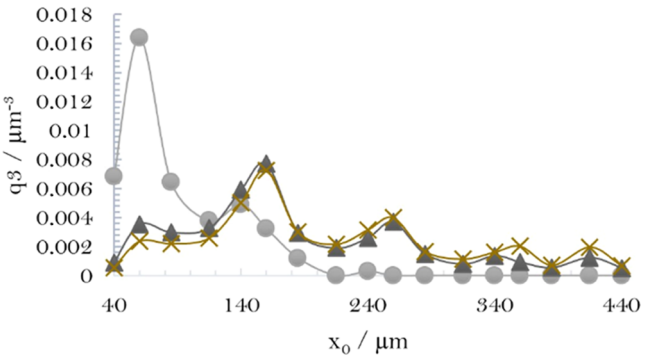

Figure 9. q_3 Distribution calculated from particle size distribution (q_0) measurements obtained from the KLOTZ particle sensor in the crystallizer product stream. Curves for three different stages of the experiment: 9 min (●, Start-up), 27 min (▲), and 30 min (×, steady-state operation). The data points for each series are connected as a guide to the eye.

Furthermore, it appears that an increase in feed rate results in a general decrease of particle residence time since the average residence time for the measurements at 10 mL min^{-1} shown in Figure 8A shows higher residence times than those shown in Figure 8B at 16 mL min^{-1}. This can be explained by the fact that an increase in feed and product withdrawal rate causes a larger zone of turbulence toward the product drain caused by the stream withdrawn from the crystallizer.

Figure 8B shows the results for the measurements at a 16 mL min^{-1} feed rate. It is clear that the maximum residence time decrease from around 60 to 50 s compared to the experiments at a lower feed rate of 10 mL min^{-1}. From the data obtained, it can be concluded that independent of the feed rate, an increase of the recirculation rate above 300 mL min^{-1} does not influence the crystallizer properties in terms of performance.

Using the data from liquid and particle RTDs, an overall estimation of the behavior of a suspension inside the crystallizer can be obtained. With residence times of 200−580 s obtained for the liquid phase it reaches approximately 5−10 times the residence times of the respective particles. This was expected since the liquid occupies the entire crystallizer, whereas the particles should only be located in the conical part. Therefore, depending upon the flow behavior inside the crystallizer, larger particles should exit the crystallizer immediately, whereas each volume fraction of liquid passes the recirculation stream and therefore remains in the crystallizer for a longer period of time than at least the larger particles, statistically spoken depending upon.

Crystallization Experiments. In order to successfully prove a stable operation of the crystallizer, several experiments were carried out using seeded crystallization and continuously tracking the evolution of the particle size distribution at the exit of the crystallizer from starting up the crystallizer till the particle size distribution remained stable, i.e., steady state was achieved. A characterization of the start-up phase is shown in Figure 9, monitoring the initial changes of the product PSD until a constant product quality is obtained.

The time point t = 0 indicates the first seed crystals entering the crystallizer. A small fraction of the seed particles leaves the crystallizer immediately through the product discharge port and the resulting PSD reflects the seed particle size distribution. The majority of particles passing the outlet remain in the crystallizer and grow. Consequently, the size

https://doi.org/10.1021/acs.oprd.3c00126
Org. Process Res. Dev. 2023, 27, 1455−1462

distribution in the product stream exhibits a shift toward larger particle sizes and the fraction of smaller particles decreases. After 20−30 min, the PSD stabilizes and steady state is reached. The supersaturation in this experiment was deliberately chosen to be rather low with only 1 °C of supersaturation (Δc = 0.5%w) with respect to the equilibrium concentration defined by the solubility curve, in order to minimize the risk of fouling inside the crystallizer. Stable steady-state operation was maintained for up to 2 h, before terminating the experiments.

The recirculation rate was set at 200 mL min^{-1}, and the feed pump was set at 50 mL min^{-1}. As already stated in the particle residence time measurements, the recirculation rate was sufficient to keep the particles suspended in the fluidized bed. The higher feed rate was chosen because cooling of the solution and therefore clogging occurred in the feed and product withdrawal tubing at lower feed rates. Improved insulation of the feed and product withdrawal tubes is required to alleviate this problem and to allow access to lower feed rates. This will be addressed in further work to be published separately. Due to the high feed rate (and therefore low residence time) and the low supersaturation, the crystal growth rate was expected to be low. Nonetheless, a significant change in particle size distribution can be observed in the online PSD measurements. Additionally, product particles were examined under the microscope and compared to the initial seed particles, as shown in Figure 10.

The seed particles are significantly smaller than the product particles and no increase in agglomeration of particles can be observed in the product. In addition, the surface of the crystals appears to be considerably smoother in the product and the typical prismatic shape of ASA can be seen. The seed crystals, in contrast, have a rough surface due to the milling and sieving process they were subjected to in order to isolate the required size fraction.

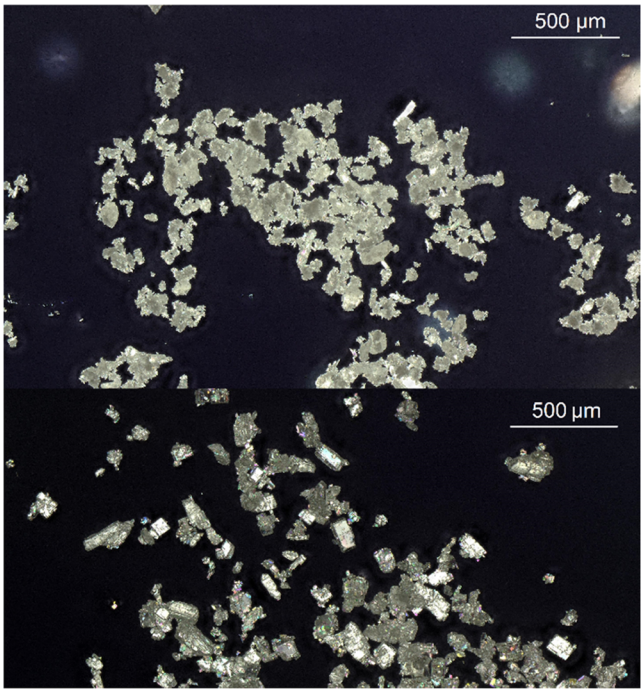

Figure 10. Comparison of the seed crystals (top) and the product crystals isolated from the product stream of the crystallizer (bottom) by means of optical microscopy. The magnification of the images is 100×; a scale bar is provided in the top right corner.

CONCLUSIONS

In this work, a novel design of a small-scale crystallizer for the continuous crystallization of pharmaceutical compounds was developed. The results of the experiments clearly demonstrate that the crystallizer is fully functional as designed and facilitates the formation of a stable fluidized bed within the conical part. It offers optional process control via control of supersaturation, and also via manipulation of the feed and recirculation flow rates. The particle size produced can be controlled by adaptation of the pump rate to increase or decrease the particle residence time and therefore the time available for crystal growth of the individual crystals in the fluidized bed.

Furthermore, it has been shown that the use of additive manufacturing not only enables flexible and tailor-made design of the crystallizer parts but also provides the possibility to adapt the geometry quickly, depending upon experimental results. This decreases the development time necessary to produce a fully functional device for crystallization. With regard to the material and production method used, it should be mentioned that the surface obtained by 3D printing is not as smooth as that of traditional glassware. Future experimental work will include different postprocessing methods such as polishing in order to gain greater insight into the influence of material properties on the performance of the crystallizer. To the best of the authors' knowledge, currently, no comparable setup manufactured using traditional materials (e.g., glassware) has been reported in the literature.

The modular build of the crystallizer facilitates fast and cheap adaptions to the design, requiring fabrication of only those parts affected by design modifications and thus reducing overall production costs and construction time in between phases of redesigning.

Even the mode of operation can be changed easily from currently cooling crystallization to other process types. Adding a mixing unit at the inlet of the feed tube provides the ability to perform antisolvent or reactive crystallization with this type of crystallizer. Evaporative crystallization appears feasible with appropriate design modifications since the material properties allow operation at elevated experimental temperatures.

In summary, the presented approach to a 3D-printed prototype for crystallization as well as the workflow needed to construct a fully functional device have been shown to be successful and promising. Future work will focus not only on a more detailed characterization of the performance of the crystallizer presented here but also on possible performance improvements accompanying a more wide-ranging redesign of the geometry of the crystallizer to unlock the potential of applying various modes of operation.

AUTHOR INFORMATION

Corresponding Authors

Nico Nys − *Institute of Process and Particle Engineering, Graz University of Technology, Graz 8010, Austria;* orcid.org/0009-0009-6403-9821; Email: nico.nys@tugraz.at

Heidrun Gruber-Woelfler − *Institute of Process and Particle Engineering, Graz University of Technology, Graz 8010, Austria; Research Center Pharmaceutical Engineering GmbH, Graz 8010, Austria;* orcid.org/0000-0002-6917-4442; Email: woelfler@tugraz.at

https://doi.org/10.1021/acs.oprd.3c00126
Org. Process Res. Dev. 2023, 27, 1455−1462

Authors

Michael König − *Institute of Process and Particle Engineering, Graz University of Technology, Graz 8010, Austria*

Peter Neugebauer − *Institute of Process and Particle Engineering, Graz University of Technology, Graz 8010, Austria; Research Center Pharmaceutical Engineering GmbH, Graz 8010, Austria;* orcid.org/0000-0002-9671-9997

Matthew J. Jones − *Thermo Fisher Scientific, Linz 4020, Austria;* orcid.org/0000-0003-1951-0708

Complete contact information is available at: https://pubs.acs.org/10.1021/acs.oprd.3c00126

Notes

The authors declare no competing financial interest.

■ ACKNOWLEDGMENTS

N.N. kindly thanks Thermo Fisher Scientific in Linz for sponsoring his PhD project, from which this publication results.

■ REFERENCES

(1) Burcham, C. L.; Florence, A. J.; Johnson, M. D. Continuous Manufacturing in Pharmaceutical Process Development and Manufacturing. *Annu. Rev. Chem. Biomol. Eng* **2018**, *9*, 253−281.

(2) Ntamo, D.; Lopez-Montero, E.; Mack, J.; Omar, C.; Highett, M. I.; Moss, D.; Mitchell, N.; Soulatintork, P.; Moghadam, P. Z.; Zandi, M. Industry 4.0 in Action: Digitalisation of a Continuous Process Manufacturing for Formulated Products. *Digital Chem. Eng.* **2022**, *3*, No. 100025.

(3) Vargas, J. M.; Nielsen, S.; Cárdenas, V.; Gonzalez, A.; Aymat, E. Y.; Almodovar, E.; Classe, G.; Colón, Y.; Sanchez, E.; Romañach, R. J. Process Analytical Technology in Continuous Manufacturing of a Commercial Pharmaceutical Product. *Int. J. Pharm.* **2018**, *538*, 167−178.

(4) Williams, J. D.; Pöchlauer, P.; Okumura, Y.; Inami, Y.; Kappe, C. O. Photochemical Deracemization of a Medicinally-Relevant Benzopyran Using an Oscillatory Flow Reactor. *Chem. - Eur. J.* **2022**, *28*, No. e202200741.

(5) Stueckler, C.; Hermsen, P.; Ritzen, B.; Vasiloiu, M.; Poechlauer, P.; Steinhofer, S.; Pelz, A.; Zinganell, C.; Felfer, U.; Boyer, S.; Goldbach, M.; De Vries, A.; Pabst, T.; Winkler, G.; Lavopa, V.; Hecker, S.; Schuster, C. Development of a Continuous Flow Process for a Matteson Reaction: From Lab Scale to Full-Scale Production of a Pharmaceutical Intermediate. *Org. Process Res. Dev.* **2019**, *23*, 1069−1077.

(6) Wernik, M.; Poechlauer, P.; Schmoelzer, C.; Dallinger, D.; Kappe, C. O. Design and Optimization of a Continuous Stirred Tank Reactor Cascade for Membrane-Based Diazomethane Production: Synthesis of α-Chloroketones. *Org. Process Res. Dev.* **2019**, *23*, 1359−1368.

(7) Znidar, D.; O'Kearney-Mcmullan, A.; Munday, R.; Wiles, C.; Poechlauer, P.; Schmoelzer, C.; Dallinger, D.; Kappe, C. O. Scalable Wolff-Kishner Reductions in Extreme Process Windows Using a Silicon Carbide Flow Reactor. *Org. Process Res. Dev.* **2019**, *23*, 2445−2455.

(8) Power, G.; Hou, G.; Kamaraju, V. K.; Morris, G.; Zhao, Y.; Glennon, B. Design and Optimization of a Multistage Continuous Cooling Mixed Suspension, Mixed Product Removal Crystallizer. *Chem. Eng. Sci.* **2015**, *133*, 125−139.

(9) Hohmann, L.; Gorny, R.; Klaas, O.; Ahlert, J.; Wohlgemuth, K.; Kockmann, N. Design of a Continuous Tubular Cooling Crystallizer for Process Development on Lab-Scale. *Chem. Eng. Technol.* **2016**, *39*, 1268−1280.

(10) Besenhard, M. O.; Neugebauer, P.; Ho, C. Da.; Khinast, J. G. Crystal Size Control in a Continuous Tubular Crystallizer. *Cryst. Growth Des.* **2015**, *15*, 1683−1691.

(11) Jiang, M.; Braatz, R. D. Designs of Continuous-Flow Pharmaceutical Crystallizers: Developments and Practice. *CrystEngComm* **2019**, 3534−3551.

(12) Eder, R. J. P.; Radl, S.; Schmitt, E.; Innerhofer, S.; Maier, M.; Gruber-Woelfler, H.; Khinast, J. G. Continuously Seeded, Continuously Operated Tubular Crystallizer for the Production of Active Pharmaceutical Ingredients. *Cryst. Growth Des.* **2010**, *10*, 2247−2257.

(13) Méndez del Río, J. R.; Rousseau, R. W. Batch and Tubular-Batch Crystallization of Paracetamol: Crystal Size Distribution and Polymorph Formation. *Cryst. Growth Des.* **2006**, *6*, 1407−1414.

(14) Alvarez, A. J.; Myerson, A. S. Continuous Plug Flow Crystallization of Pharmaceutical Compounds. *Cryst. Growth Des.* **2010**, *10*, 2219−2228.

(15) Lawton, S.; Steele, G.; Shering, P.; Zhao, L.; Laird, I.; Ni, X. W. Continuous Crystallization of Pharmaceuticals Using a Continuous Oscillatory Baffled Crystallizer. *Org. Process Res. Dev.* **2009**, *13*, 1357−1363.

(16) Sonnenschein, J.; Heming, R.; Wohlgemuth, K. Archimedes Tube Crystallizer: Design and Operation of Continuous Cooling Crystallization Based on First-Principle Modeling. *Cryst. Growth Des.* **2022**, *22*, 5272−5284.

(17) Etmanski, M. M.; Breloer, M.; Weber, M.; Schembecker, G.; Wohlgemuth, K. Interplay of Particle Suspension and Residence Time Distribution in a Taylor−Couette Crystallizer. *Crystals* **2022**, *12*, No. 1845.

(18) Mothes, H. No-Regret Solutions - Modular Production Concepts in Times of Complexity and Uncertainty. *Chem. Ing. Tech.* **2015**, *87*, 1159−1172.

(19) Gutmann, B.; Köckinger, M.; Glotz, G.; Ciaglia, T.; Slama, E.; Zadravec, M.; Pfanner, S.; Maier, M. C.; Gruber-Wölfler, H.; Oliver Kappe, C. Design and 3D Printing of a Stainless Steel Reactor for Continuous Difluoromethylations Using Fluoroform. *React. Chem. Eng.* **2017**, *2*, 919−927.

(20) Maier, M. C.; Lebl, R.; Sulzer, P.; Lechner, J.; Mayr, T.; Zadravec, M.; Slama, E.; Pfanner, S.; Schmölzer, C.; Pöchlauer, P.; Kappe, C. O.; Gruber-Woelfler, H. Development of Customized 3D Printed Stainless Steel Reactors with Inline Oxygen Sensors for Aerobic Oxidation of Grignard Reagents in Continuous Flow. *React. Chem. Eng.* **2019**, *4*, 393−401.

(21) Meise, M.; Jäger, L.; Wilk, A.; Heitmann, T.; Scholl, S. Residence Time Characteristics of the Novel Archimedean Screw Crystallizer/Reactor. *Chem. Ing. Tech.* **2020**, *92*, 1074−1082.

(22) Li, C.; Ding, B.; Zhang, L.; Song, K.; Tao, S. 3D-Printed Continuous Flow Reactor for High Yield Synthesis of CH3NH3PbX3 (X = Br, I) Nanocrystals. *J. Mater. Chem. C* **2019**, *7*, 9167−9174.

(23) Lewis, J. A.; Smay, J. E.; Stuecker, J.; Cesarano, J. Direct Ink Writing of Three-Dimensional Ceramic Structures. *J. Am. Ceram. Soc.* **2006**, *89*, 3599−3609.

(24) Myerson, A. S.; Erdemir, D.; Lee, A. Y.*Handbook of Industrial Crystallization*; Cambridge University Press, 2019; pp 1−528.

(25) Chianese, A.; Kramer, H. J. M. *Industrial Crystallization Process Monitoring and Control*; Wiley-VCH, 2012.

(26) Orehek, J.; Teslić, D.; Likozar, B. Continuous Crystallization Processes in Pharmaceutical Manufacturing: A Review. *Org. Process Res. Dev.* **2021**, 16−42.

(27) Maia, G. D.; Giulietti, M. Solubility of Acetylsalicylic Acid in Ethanol, Acetone, Propylene Glycol, and 2-Propanol. *J. Chem. Eng. Data* **2008**, *53*, 256−258.

(28) Maier, M. C.; Valotta, A.; Hiebler, K.; Soritz, S.; Gavric, K.; Grabner, B.; Gruber-Woelfler, H. 3D Printed Reactors for Synthesis of Active Pharmaceutical Ingredients in Continuous Flow. *Org. Process Res. Dev.* **2020**, *24*, 2197−2207.

(29) Ruprecht, N. A.; Kohlus, R. *Determination and Modelling of the Particle Size Dependent Residence Time Distribution in a Pilot Plant Spray Dryer*, Proceedings of 21th International Drying Symposium; Universitat Politecnica de Valencia, 2019.

(30) Levenspiel, O. *Chemical Reaction Engineering*, 3rd ed.; Anderson, W.; Santor, K., Eds.; John Wiley & Sons: New York, 1999.